International Journal of Computational and Experimental Science and ENgineering (IJCESEN)

Vol. 10-No.4 (2024) pp. 1712-1718
http://www.ijcesen.com

ISSN: 2149-9144

Research Article

Multi-Layer Absorber based on Plasmonic Resonances for Photovoltaic Applications at Visible Spectra

Yasemin Demirhan[1,2*]

[1]Department of Physics, Izmir Institute of Technology, 35430 Urla, Izmir, Turkey
[2]Center for Materials Research, Integrated Research Centers, IZTECH, 35430 Urla, Izmir, Turkey
* **Corresponding Author Email:** yasemindemirhan@iyte.edu.tr- **ORCID:** 0000-0002-7782-4468

Article Info:

DOI: 10.22399/ijcesen.778
Received : 16 December 2024
Accepted : 23 December 2024

Keywords :

Solar Cell Absorbers,
Metamaterials,
Wide-angle Absorbers,

Abstract:

This paper introduces a broadband absorber based on a multilayered, double-cylindrical-shaped metamaterial, numerically characterized for its performance. The structure comprises four interacting layers that generate plasmonic resonances. CST microwave simulations were conducted to analyze its absorption characteristics. The results demonstrate that the proposed metamaterial absorber achieves 99% absorption at 847 nm frequency region and 98% absorption in the 500-1200 nm frequency region. Additionally, polarization dependency analysis confirms that the absorber performs as a perfect, polarization-independent absorber across the studied frequency range. It exhibits high absorption in both TE and TM modes and remains unaffected by polarization or variations in the incident angle. Numerical simulations reveal that the absorption performance is driven by a combination of Fabry–Perot resonance effects, localized surface plasmons, and propagating surface plasmons. In summary, the proposed metastructure demonstrates omnidirectional absorption, polarization independence, and wide-angle incident absorption. This design shows significant potential for applications in photodetectors, active optoelectronic devices, and sensors.

1. Introduction

Solar energy is an exceptional renewable energy resource that generates electricity by the help of photovoltaic (PV) cells [1]. The amount of energy achieved from the electromagnetic (EM) radiation within a single hour can satisfy the annual energy demand of the world. Therefore, the latest researches are aimed to design solar absorbers with high efficiency with an ease of fabrication [2]. Solar absorbers, are crucial elements affecting the performance of solar photovoltaic systems. An optimum solar absorber should have high absorbance characteristic in a wide spectral range from UV to near-infrared, where the most of solar energy takes place [3]. Besides, zero emittance property in the mid-infrared is required to minimize the heat loss from self-emission. So, perfect wideband solar absorption and low mid-infrared emission are the most important features for a high efficiency solar absorber. Perfect absorption, an excellent opportunity is related to field localization, has many potential applications such as, energy harvesting [4,5], light emitting diodes [6,7], sensing [8–10], and optical filters [11,12]. Different type of design structures have been studied to absorb specific regimes of electromagnetic waves, including visible [13,14], infrared [15], terahertz [16], and gigahertz [17]. Especially, these designs includes three separate layers: a top layer, a dielectric spacer, and a metallic substrate that forming a metallic sub-wavelength resonator [18,19]. The absorption characteristics mainly effect from the geometric parameters of the design. The optical and electrical features of the designed absorber can be adjust mainly by tuning the design configuration [20].

Photovoltaic (PV) solar cell is a kind of non-mechanical device that can directly convert sunlight into electricity. It is well known that there is an absorption and re-emission mechanism in photovoltaic cells. Thus, the perfect plasmonic absorbers has to absorb solar radiation in a wide range to enhance the solar energy efficiency [21]. In addition, independence of the polarization state is also a key character to increase the absorption of the solar energy. Recently, the researchers focused on metamaterial solar absorbers that can provide

selective absorption or emission by exciting plasmonic resonances at particular wavelengths [22, 23]. Metamaterial is a kind of artificial material that can be designed for the desired wavelength naturally consists of periodic unitcell structure. The permeability and permittivity of metamaterial can be designed simultaneously, therefore it has a wide range of applications in the field of light capture and manipulation by tailoring both phase and amplitude on the subwavelength range [24-27]. Since the first demonstration of the metamaterials, a huge number of ultrathin, highly integrated optical devices have been studied for applications as; flat metalens [28], beam splitters [29], polarization conversion devices [25], perfect absorbers [30].

Perfect absorption can be achieved when the frequency-dependent effective impedance of the metamaterial absorber is the same as the impedance of free spaces where reflected and transmitted waves drop to zero [31]. The resonance frequency and efficiency of metamaterial absorbers are highly dependent on the geometric design parameters of the structure. By varying these parameters; the electrical and optical behavior of such plasmonic absorbers have gain tunable characteristic and can be easily optimized and initiated [32].

Previous studies have reported various absorber designs operating in the visible range, but each faced notable limitations. For instance, Ullah et al. [33] developed a multiband absorber that achieved only 50% absorption efficiency. Mulla et al. [34] introduced a polarization-independent multiband absorber, but the resonance width was restricted to just 34 nm. In summary, while perfect absorbers with an average absorption of 94% and dual-band absorbers [34] have been investigated, these designs either displayed significant angle-dependence or had narrow resonance widths, limiting their practical usability. Thus, there is a need of design and fabricate a wide-angle, polarization-independent, selective solar absorbers with high absorptance from UV to near-infrared region.In this work, we design numerically studied metamaterial structures made of double cylindrical cones which has the ability of perfect absorbtion. The metamaterial absorber exhibits absorption greater than 95% from 500 nm to 1500 nm frequency region, and an average absorption of 94 % is also achieved between 500 nm to 3500 nm.

2. Material and Methods

2.1 Geometry and Simulation Method

We have designed a unique geometry that composed of cylindrical shaped binary mesa structure combining with a multi-layer film structure, to realize a perfect absorber from visible light to near infrared band. The unitcell consists of a ground-plane layer {300 nm x 300 nm gold layer (h1) and 300 nm x 300 nm silicone layer (h2)}, nickel layer {300 nm x 300 nm (h3)}, cyclindrical pillar a {200 nm diameter silicone (h4) and 200 nm diameter nickel (h5)}, cyclindrical pillar b {120 nm diameter silicone (h6) and 120 nm diameter nickel (h7)}. Through parameter optimization by CST simulations, the height parameters of the metamaterial structure are set to h1=200 nm, h2 = 150 nm, h3 = 30 nm, h4 = 150 nm, h5 = 20 nm, h6 = 150 nm, h7= 20 nm. The thickness of the silicon which is used as a dielectric layer is h2 = 150 nm, that is sufficient for absorption at shorter wavelengths), the thickness of the metallic substrate that is used as a reflector to reduce the transmission is h1 = 200 nm. At shorter wavelengths, the metallic component plays a more significant role due to increased Ohmic losses and plasmon decay. In solar cell applications, where the metallic substrate primarily absorbs light, a P-type semiconductor can be placed beneath the substrate. In the absence of light, some free electrons from the metallic substrate diffuse into the semiconductor, forming a PN junction due to the charge imbalance at the interface. In the simulation, the dielectric constant of SiO_2 is 1.45, and the dielectric constants of Ni and Au can be obtained from material library of CST microwave studio. Because the thickness of the metallic Au layer is greater than its skin depth, transmittance is negligible.

In figure 1., the schematic diagram of metamaterial structure with perspective view, numerical analysis setup and conceptual layout is given.

3. Results and Discussions

The proposed metastructure leverages two primary mechanisms: Fabry–Perot Resonances and the plasmonic effects. The multilayer configuration enhances absorption at target frequencies by creating standing waves through constructive interference, a phenomenon explained by Fabry–Perot resonance. Additionally, plasmonic effects, driven by localized surface plasmons (LSPs) and propagating surface plasmons (PSPs) induced at the interfaces, trap incident light and convert it into localized energy, further boosting the absorber's All computations and numeric analysis are performed using CST Microwave Studio software. The simulation domain is subjected to Floquet periodic boundary conditions, which ensure the periodic repetition of the unit cells in both the x- and y-directions. The effect of geometric

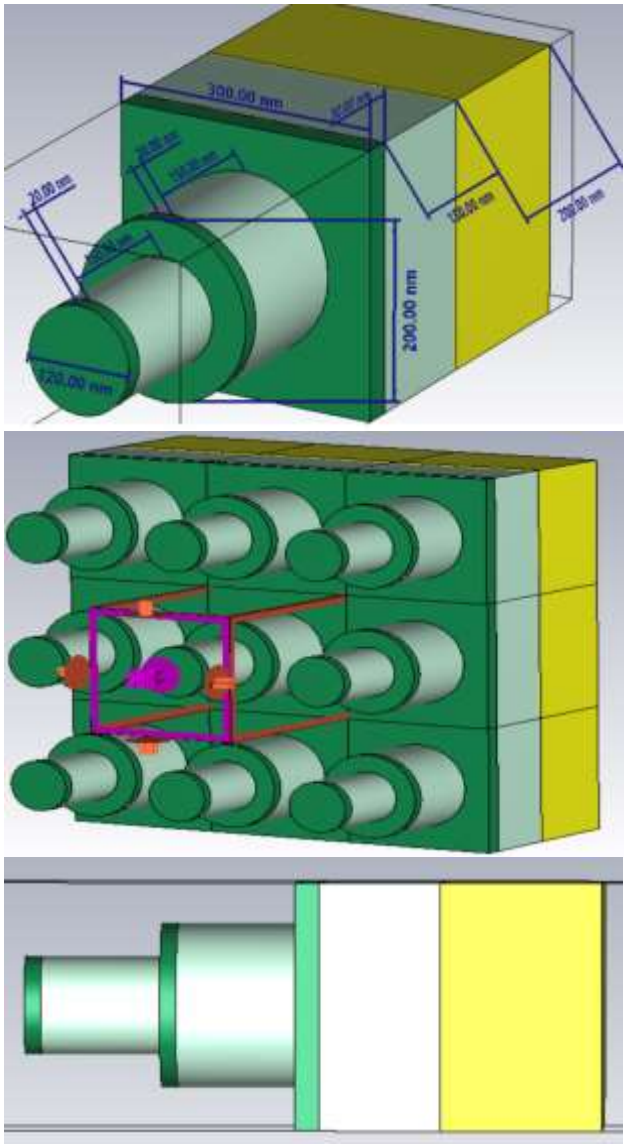

Figure 1. *Schematic diagram of metamaterial structure with (a) perspective view , and (d) numerical analysis setup. (c) conceptual layout*

dimensions on the absorption performance of the metamaterial structure was investigated through simulations, focusing on variations in cylindrical pillar height and incident angle. The absorption performance was then analyzed for both single and double-pillar configurations, highlighting the influence of the binary pillar structure. We also investigate the effect of surface plasmon waves (SPWs) within the absorber by E-field and H-field monitoring. efficiency [35]. CST simulations were conducted to examine the frequency-dependent absorption characteristics, optimize geometric parameters, and evaluate the impact of polarization on absorption efficiency. Figure 2 shows the absorption spectra of the proposed metamaterial structure with double mesa pillar design. The proposed mesa pillar structure exhibits ultra-broadband absorption exceeding 95% across

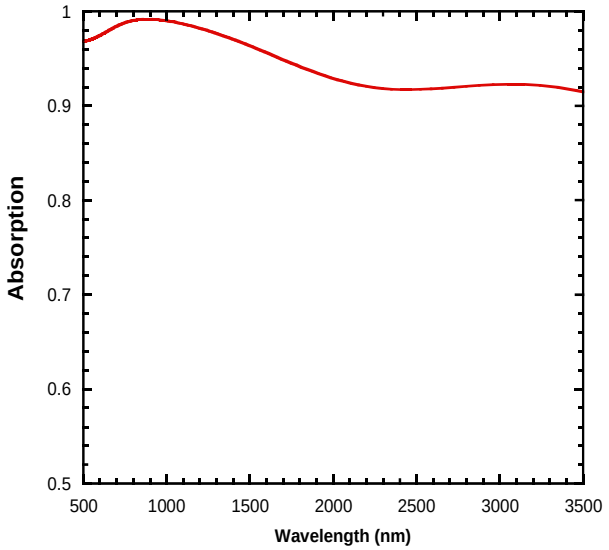

Figure 2. *The absorption spectrum of the proposed mesa pillar structure (double mesa pillar design).*

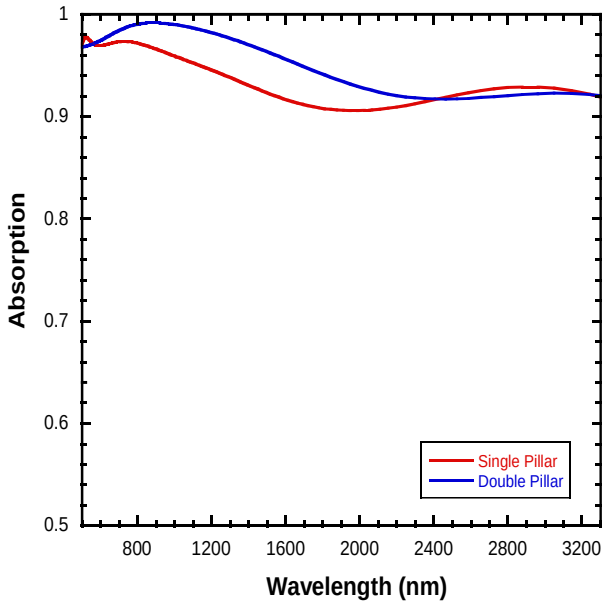

Figure 3. *The absorption spectrum of the proposed mesa pillar structure with single mesa and double mesa design on the same graph.*

wavelengths ranging from 500 nm to 3300 nm, with an average absorption of up to 98.7 % within this range. Notably, peak absorption reaches 98 % in 210 nm and 99.4 % accross the wavelengths ranging from 830–1040 nm and 2020–2433 nm. To highlight the effect of the double mesa structure on the absorber, the single mesa structure was also analyzed and plotted on the same graph (figure 3). In figure 3., the absorption spectrum of the proposed mesa pillar structure with single mesa and double mesa design are given on the same plot. For the single mesa structure, the maximum absorption reaches up to 97% at 520 nm and 92% in the range

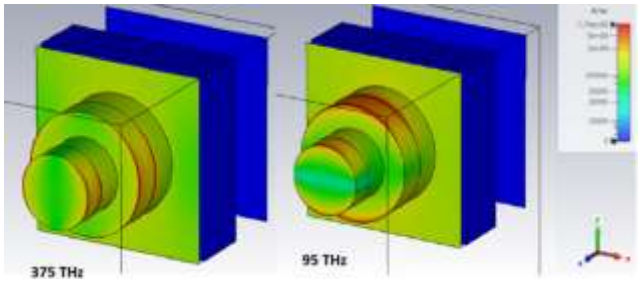

E-Field (Perspective View)

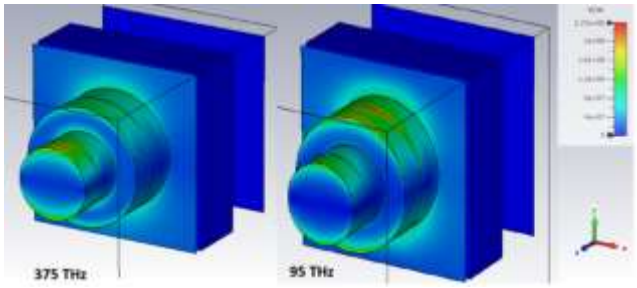

H-Field (Perspective View)

Figure 4. *E-field and H-field distributions at TE mode.*

of 2500 nm to 3200 nm. Notably, the proposed absorber structure exhibits significantly enhanced absorption efficiency in the range of 500 nm to 2200 nm compared to the single-grating structure. However, beyond 2200 nm, its absorption exceeds that of the double mesa structure. Consequently, the double mesa structure demonstrates weaker absorption in the longer wavelength region.

Figure 4 illustrates the E-field and H-field distributions for the TE mode, providing a perspective view of the electromagnetic interactions within the structure (for 95 THz and 375 THz). The E-field distribution demonstrates a strong localization near the edges of the metallic components and within the air gaps, highlighting the dominance of electric resonance effects. This suggests efficient confinement and coupling of electric energy in the designed metamaterial. In contrast, the H-field distribution shows a relatively smoother spread, with weaker intensity compared to the E-field. This indicates that magnetic contributions are less pronounced in driving the observed absorption characteristics. Together, these distributions confirm that the broadband absorption mechanism is primarily influenced by the electric field resonances, with the magnetic field playing a secondary role.

In figure 5, the absoption spectrum of the mesa pillar structure via different cyclindrical mesa pillar a (h4) thicknesses are shown. As the thickness of the mesa pillar (h4) increases from 150 nm to 210 nm, the absorption in the longer wavelength range significantly increases, while the absorption in the

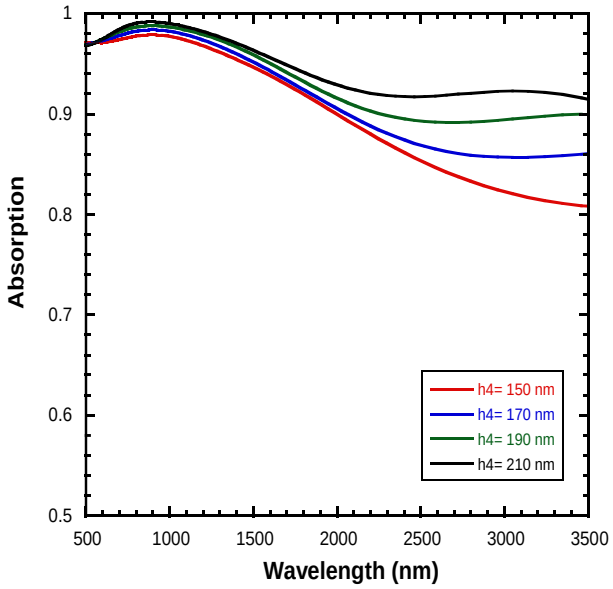

Figure 5. *The absorption spectrum of the proposed mesa pillar structure with varying cyclindrical mesa pillar a (h4) thickness.*

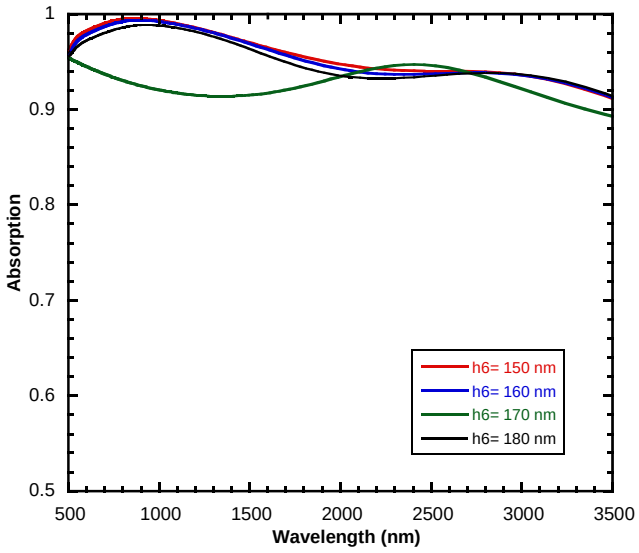

Figure 6. *The absorption spectrum of the proposed mesa pillar structure with varying cyclindrical mesa pillar b (h6) thickness.*

shorter wavelength range slightly increases. After considering the bandwidth and absorption efficiency, the optimal thickness of h4 is chosen to be 210 nm.As the final step in parameter optimization, the impact of the cylindrical mesa pillar thickness (h6) is analyzed (figure 6). When the mesa pillar thickness (h6) increases from 150 nm to 180 nm, absorption in the 500–3000 nm wavelength range shows a slight decrease, while absorption above 3000 nm remains largely unaffected. However, at 180 nm, a significant reduction in absorption is observed in the shorter wavelength region, along with notable variations in absorption characteristics. These results suggest

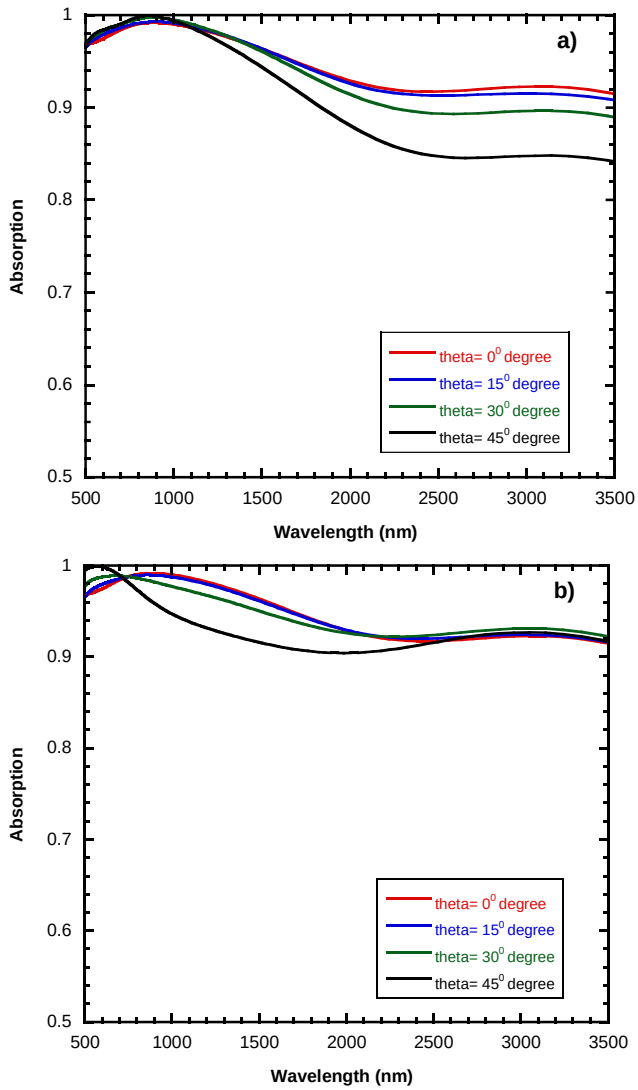

Figure 7. *Absorption spectra with incident angle tuning from 0^0 to 45^0 (a) TE polarization (b) TM polarization.*

that the optimal thickness for h6 is 150 nm for this design. In practical applications, the effect of the incident angle on the absorption spectrum must be considered. The absorption spectra for different incident incidences are calculated and shown in Figures 7(a) and 7(b), with the incident angle varying from 0° to 45°. For TM-polarized light, the absorption bandwidth exhibits a blue shift; however, it maintains an absorption rate exceeding 90% across the 500–3000 nm range, even at an incident angle of 45°. Significantly, within the crucial 500–700 nm range, particularly relevant for solar cell applications, the absorption peaks at 99% under the same conditions. For TE-polarized light, the absorption gradually decreases but maintains an average of approximately 85% across the 500–3500 nm range, even at a 45° incident angle. Furthermore, the absorption peaks exhibit a slight blue shift, attributed to the decrease in the effective refractive index of the binary grating with increasing incident angle. These findings highlight the proposed absorber's robustness and minimal sensitivity to changes in the incident angle. Consequently, the proposed mesa pillar design demonstrates high absorption across all incident angles, showcasing its effectiveness for wide-incident-angle applications.

The results indicate that the absorber meets the expected performance criteria, successfully absorbing a broad range of visible and near-infrared wavelengths. This characteristic makes it suitable for use as a wideband band-stop filter with tunability. Additionally, the structure can be applied in mid-infrared cameras to eliminate unwanted visible and near-infrared background interference, enhancing image clarity and functionality.

4. Conclusions

This paper presents a multilayer, double-cylindrical metamaterial absorber that achieves near-perfect absorption across a broad spectrum in the visible range. Numerical simulations reveal its exceptional performance, featuring omnidirectional absorption, polarization independence, and wide-angle functionality. By leveraging a combination of Fabry–Perot resonance and plasmonic effects, the proposed design demonstrates remarkable absorption efficiency. These properties make it a highly promising solution for next-generation solar energy harvesting and advanced optoelectronic applications.

Author Statements:

- **Ethical approval:** The conducted research is not related to either human or animal use.
- **Conflict of interest:** The authors declare that they have no known competing financial interests or personal relationships that could have appeared to influence the work reported in this paper
- **Acknowledgement:** The authors declare that they have nobody or no-company to acknowledge.
- **Author contributions:** The authors declare that they have equal right on this paper.
- **Funding information:** The authors declare that there is no funding to be acknowledged.
- **Data availability statement:** The data that support the findings of this study are available on request from the corresponding author. The data are not publicly available due to privacy or ethical restrictions.

References

[1] Lee, T. D., & Ebong, A. U. (2017). A review of thin film solar cell technologies and challenges. *Renewable and Sustainable Energy Reviews*, *70*, 1286-1297. https://doi.org/10.1016/j.rser.2016.12.028

[2] Ranabhat, K., Patrikeev, L., Revina, A. A. E., Andrianov, K., Lapshinsky, V., & Sofronova, E. (2016). An introduction to solar cell technology. *Journal of Applied Engineering Science*, *14*(4). DOI:10.5937/JAES14-10879

[3] Carron, R., Andres, C., Avancini, E., Feurer, T., Nishiwaki, S., Pisoni, S., ... & Tiwari, A. N. (2019). Bandgap of thin film solar cell absorbers: A comparison of various determination methods. *Thin Solid Films*, *669*, 482-486. https://doi.org/10.1016/j.tsf.2018.11.017

[4] Xiao, T., Tu, S., Liang, S., Guo, R., Tian, T., & Müller-Buschbaum, P. (2023). Solar cell-based hybrid energy harvesters towards sustainability. *Opto-Electronic Science*, *2*(6), 230011-1.

[5] Guo, C. X., Guai, G. H., & Li, C. M. (2011). Graphene based materials: enhancing solar energy harvesting. *Advanced Energy Materials*, *1*(3), 448-452.

[6] Lo, S. C., & Burn, P. L. (2007). Development of dendrimers: Macromolecules for use in organic light-emitting diodes and solar cells. *Chemical Reviews*, *107*(4), 1097-1116.

[7] Wang, F., Liu, X. K., & Gao, F. (2019). Fundamentals of solar cells and light-emitting diodes. In *Advanced nanomaterials for solar cells and light emitting diodes* (pp. 1-35). Elsevier.

[8] Tang, J., Xiao, Z., & Xu, K. (2016). Ultra-thin metamaterial absorber with extremely bandwidth for solar cell and sensing applications in visible region. *Optical Materials*, *60*, 142-147.

[9] Asaba, K., Moriyama, K., & Miyamoto, T. (2022, November). Preliminary Characterization of Robust Detection Method of Solar Cell Array for Optical Wireless Power Transmission with Differential Absorption Image Sensing. In *Photonics* 9(11); 861).

[10] Manikandan, P. N., Imran, H., & Dharuman, V. (2019). Self-powered polymer–metal oxide hybrid solar cell for non-enzymatic potentiometric sensing of bilirubin. *Medical Devices & Sensors*, *2*(2), e10031.

[11] Almarzooqi, N. K., Ahmad, F. F., Hamid, A. K., Ghenai, C., Farag, M. M., & Salameh, T. (2023). Experimental investigation of the effect of optical filters on the performance of the solar photovoltaic system. *Energy Reports*, *9*, 336-344.

[12] Taylor, R. A., Otanicar, T., & Rosengarten, G. (2012). Nanofluid-based optical filter optimization for PV/T systems. *Light: Science & Applications*, *1*(10), e34-e34.

[13] Mudachathi, R., & Tanaka, T. (2018). Broadband plasmonic perfect light absorber in the visible spectrum for solar cell applications. *Advances in Natural Sciences: Nanoscience and Nanotechnology*, *9*(1), 015010.

[14] Gao, H., Peng, W., Liang, Y., Chu, S., Yu, L., Liu, Z., & Zhang, Y. (2020). Plasmonic broadband perfect absorber for visible light solar cells application. *Plasmonics*, *15*, 573-580.

[15] Sargent, E. H. (2009). Infrared photovoltaics made by solution processing. *Nature Photonics*, *3*(6), 325-331.

[16] Hempel, H., Savenjie, T. J., Stolterfoht, M., Neu, J., Failla, M., Paingad, V. C., & Unold, T. (2022). Predicting solar cell performance from terahertz and microwave spectroscopy. *Advanced Energy Materials*, *12*(13), 2102776.

[17] Maurya, V., & Singhal, S. (2024). Solar energy harvesting using nanostructured ultrawideband absorber with nearly perfect thermal emission. *Solar Energy Materials and Solar Cells*, *277*, 113126.

[18] Qasrawi, A. F., & Daragme, R. B. (2022). Fabrication and characterization of Se/WO3 heterojunctions designed as terahertz/gigahertz dielectric resonators. *Optik*, *255*, 168719.

[19] Patel, S. K., Charola, S., Parmar, J., & Ladumor, M. (2019). Broadband metasurface solar absorber in the visible and near-infrared region. *Materials Research Express*, *6*(8), 086213.

[20] Du John, H. V., Sagayam, K. M., Jose, T., Pandey, D., Pandey, B. K., Kotti, J., & Kaur, P. (2023). Design simulation and parametric investigation of a metamaterial light absorber with tungsten resonator for solar cell applications using silicon as dielectric layer. *Silicon*, *15*(9), 4065-4079.

[21] Omelyanovich, M., Ra'di, Y., & Simovski, C. (2015). Perfect plasmonic absorbers for photovoltaic applications. *Journal of Optics*, *17*(12), 125901.

[22] Wang, H., & Wang, L. (2013). Perfect selective metamaterial solar absorbers. *Optics express*, *21*(106), A1078-A1093.

[23] Yu, P., Besteiro, L. V., Huang, Y., Wu, J., Fu, L., Tan, H. H., ... & Wang, Z. (2019). Broadband metamaterial absorbers. *Advanced Optical Materials*, *7*(3), 1800995.

[24] Lin, K. T., Lin, H., Yang, T., & Jia, B. (2020). Structured graphene metamaterial selective absorbers for high efficiency and omnidirectional solar thermal energy conversion. *Nature communications*, *11*(1), 1389.

[25] Noori, A., Akyürek, B., Demirhan, Y., Özyüzer, L., Güven, K., Altan, H., & Aygün, G. (2023). Terahertz wavefront engineering using a hard-coded metasurface. *Optical and Quantum Electronics*.

[26] Zeybek, S., Demirhan, Y., Noori, A., Tugay, H., Altan, H., Sabah, C., & Ozyuzer, L. (2023). Investigation of resonant properties of metamaterial THz filters fabricated from vanadium dioxide thin films. *Modern Physics Letters B*.

[27] Demirhan, Y., Alaboz, H., Nebioglu, M. A., Mulla, B., Akkaya, M., Altan, H., & Ozyuzer, L. (2017). Fourcross shaped metamaterial filters fabricated from high temperature superconducting YBCO and

Au thin films for terahertz waves. *Supercond. Sci. Technol.* 30;074006 DOI 10.1088/1361-6668/aa6fbe

[28] Li, T., Chen, C., Xiao, X., Chen, J., Hu, S., & Zhu, S. (2023). Revolutionary meta-imaging: from superlens to metalens. *Photonics Insights*, *2*(1), R01-R01.

[29] Xing, X., Li, Y., Lu, Y., Zhang, W., Zhang, X., Han, J., & Zhang, W. (2019). Terahertz metamaterial beam splitters based on untraditional coding scheme. *Optics Express*, *27*(20), A1627-A1635.

[30] Yu, P., Besteiro, L. V., Wu, J., Huang, Y., Wang, Y., Govorov, A. O., & Wang, Z. (2018). Metamaterial perfect absorber with unabated size-independent absorption. *Optics Express*, *26*(16), 20471-20480.

[31] Landy, N. I., Sajuyigbe, S., Mock, J. J., Smith, D. R., & Padilla, W. J. (2008). Perfect metamaterial absorber. *Physical review letters*, *100*(20), 207402.

[32] Kim, J., Han, K., & Hahn, J. W. (2017). Selective dual-band metamaterial perfect absorber for infrared stealth technology. *Scientific reports*, *7*(1), 1-9.

[33] Ullah, H., Khan, A. D., Noman, M., & Rehman, A. U. (2018). Novel multi-broadband plasmonic absorber based on a metal-dielectric-metal square ring array. *Plasmonics*, *13*, 591-597.

[34] Mulla, B., & Sabah, C. (2016). Multiband metamaterial absorber design based on plasmonic resonances for solar energy harvesting. *Plasmonics*, *11*, 1313-1321. https://doi.org/10.1007/s11468-015-0177-y

[35] Mizuno, T., Takeuchi, K., Kaneshima, K., Ishii, N., Kanai, T., & Itatani, J. (2019). Resonant-Like Field Enhancement by Nanoscale Grating-Coupled Propagating Surface Plasmons and Localized Surface Plasmons in the Mid-Infrared Range: Implications for Ultrafast Plasmonic Electron Sources. *ACS Applied Nano Materials*, *2*(11), 7067-7073. 10.1021/acsanm.9b01597